Dynamics of particles around a pseudo-Newtonian Kerr black hole with halos*

Wang Ying(王 颖) and Wu Xin(伍 歆)†

Department of Physics, Nanchang University, Nanchang 330031, *China*

(Received 18 November 2011; revised manuscript received 9 December 2011)

The regular and chaotic dynamics of test particles in a superposed field between a pseudo-Newtonian Kerr black hole and quadrupolar halos is detailed. In particular, the dependence of dynamics on the quadrupolar parameter of the halos and the spin angular momentum of the rotating black hole is studied. It is found that the small quadrupolar moment, in contrast with the spin angular momentum, does not have a great effect on the stability and radii of the innermost stable circular orbits of these test particles. In addition, chaos mainly occurs for small absolute values of the rotating parameters, and does not exist for the maximum counter-rotating case under some certain initial conditions and parameters. This means that the rotating parameters of the black hole weaken the chaotic properties. It is also found that the counter-rotating system is more unstable than the co-rotating one. Furthermore, chaos is absent for small absolute values of the quadrupoles, and the onset of chaos is easier for the prolate halos than for the oblate ones.

Keywords: pseudo-Newtonian potential, Kerr black hole, chaos

PACS: 05.45.–a, 04.70.–s **DOI:** 10.1088/1674-1056/21/5/050504

1. Introduction

General relativity is a highly nonlinear theory, which provides a rich source of various nonlinear phenomena. A number of examples regarding chaos, one of the nonlinear phenomena, are often visible in relativistic astrophysics.[1−5] General relativistic effects make two fixed relativistic black holes[6] or a Schwarzschild black hole plus a dipolar shell[7] have a chaotic behavior, which does not exist in the Newtonian theory of gravity. The chaotic motion of test particles in superposed Weyl spacetime such as the black hole-disk (halo, shell, or ring) configuration[8] is investigated so that some physical properties and structures associated with fields can be understood clearly. The authors of Ref. [9] surveyed the chaotic motion of charged particles in an electromagnetic field surrounding a rotating black hole, and found that the chaotic properties depend on the black hole spin. Namely, the chaotic properties are weakened by the dragging effect of the Kerr black hole. However, the spin effect is an important source for causing chaos in some other gravitational problems. For instance, there are chaotic orbits for larger[10] or smaller[11] spin values in the motion of spinning test particles around a Schwarzschild spacetime. Without doubt, the motion of spinning test particles around the Kerr spacetime should be chaotic for certain initial conditions and parameters.[12] Recently, whether chaos exists in the spinning compact binaries or not has been a hot topic.[13] The chaos in the binary systems has been confirmed by several independent groups. The above-mentioned examples belong to the chaotic geodesic or nongeodesic motion of particles in given gravitational fields. In addition, the chaotic evolution of the gravitational field itself, such as the mixmaster cosmology[14] and a closed Friedman–Robertson–Walker cosmological scalar field,[15] is considered.

It should be noted that most of the dynamical equations considered above are taken from the mathematical complexity of full general relativistic equations or post-Newtonian approximate equations. Instead, a simpler method for avoiding the complexity uses nonrelativistic equations given by the corresponding pseudo-Newtonian potential, which can keep some relativistic effects of the geometry of spacetime. The Paczyński–Wiita (PW) pseudo-Newtonian potential is a simple accurate model that mimics the positions of both the last stable circular orbit and the marginally bound circular orbit for a Schwarzschild black hole.[16] Just like in the Schwarzschild black hole plus a dipolar halo, the existence of chaos in the PW pseudo-

*Project supported by the National Natural Science Foundation of China (Grant Nos. 10873007, 11173012, and 11178002).

†Corresponding author. E-mail: xwu@ncu.edu.cn

© 2012 Chinese Physical Society and IOP Publishing Ltd

Newtonian potential plus a dipolar halo[17] also shows that the PW potential has general relativistic effects. The dynamics of the pseudo-Newtonian Hill problem is also discussed.[18] Moreover, there are several pseudo-Newtonian potentials that model the general relativistic effects on the accretion disks around Kerr black holes. Some of them are the Smerák–Karas potential,[19] the Mukhopadhyay potential,[20] and the Artemova–Björnsson–Novikov (ABN) potential.[21] In particular, the ABN potential has the least stable and marginally bound orbits in accord with those of the Kerr metric, and seems like a natural extension of the PW potential. Because of its advantages, the stability of orbits around a spinning body in the ABN pseudo-Newtonian Hill problem has been investigated in Ref. [22], where it was shown that the counter-rotating system is more unstable than the co-rotating system.

It is worth pointing out that for the ABN pseudo-Newtonian potential instead of the general relativistic solution, it is very easy to obtain a superposed gravitational field between the ABN pseudo-Newtonian potential and other gravitational fields. In this sense, it is simple to solve the geodesic equations. Above all, the ABN potential can basically model the general relativistic effects of the exact relativistic Kerr metric. Because of these advantages, in this paper we will use a quadrupolar halo and the ABN potential to compose a new gravitational field as an approximation to the exact general relativistic system consisting of the quadrupolar halo and the Kerr black hole. It is desired to know whether the ABN pseudo-Newtonian potential holds basic properties that are similar to those of the general relativistic solution from a dynamical point of view. That is to say, a main concern is to know how both the spin angular momentum of the rotating black hole and the quadrupolar parameter of the halo affect the dynamics of particles in the new field. It is expected to show that the simpler model (11) as well as the more complicated system of Ref. [9] is well suitable for the description of the rotating parameter that weakens the chaotic properties. Additionally, it is hoped to show that the effects of the spin parameter on the stability of orbits in the simpler model are basically the same as those in the pseudo-Newtonian Hill problem,[22] though there is an explicit difference between them.

This paper is organized as follows. In Section 2 we will introduce the construction of a superposed gravitational field between a pseudo-Newtonian Kerr black hole and quadrupolar halos. Then we make detailed analysis for the dynamics of a particle's circular and generic trajectories by using the following methods: Poincaé maps, Lyapunov exponents, power spectrum analysis, and fast Lyapunov indicators (FLIs). The dynamical dependence on both the spin angular momentum of the rotating black hole and the quadrupolar parameter of the halo is given in Section 3. Moreover, some of the results are explained. Finally, the summary and remarks follow in Section 4.

2. A superposed gravitational field between a pseudo-Newtonian Kerr black hole and quadrupolar halos

In general, it is difficult to accurately describe a gravitational field between a rotating black hole and the quadrupolar moment of the external distribution of matter such as a halo from a framework of rigorous general relativity. In principle, a superposed Weyl solution can be used to mimic it. However, the description of the Kerr field itself is not an easy task. A simple method uses the ABN potential as a certain approximation to the exact relativistic Kerr spacetime. The potential is a function of the radius $r = |\boldsymbol{r}|$ in the following form:

$$\phi_{\rm ABN} = -\frac{GM}{(\beta-1)r_1}\left[\left(\frac{r}{r-r_1}\right)^{\beta-1} - 1\right], \quad (1)$$

where G and M stand for the gravitational constant and the mass of the compact body, respectively. The position of the event horizon, r_1, is written as

$$r_1 = [1 + (1-a^2)^{1/2}]r_{\rm g}, \quad (2)$$

where $r_{\rm g} = GM/c^2$ is the gravitational radius with c being the speed of light, a is the spin parameter of the rotating black hole and $a \in [-1, 1)$. It should be noted that the limit case of $a = 1$ should be excluded because expression (1) converts into the Newtonian expression so that it does not mimic any spin and relativistic effects. This is analogous to the angular momentum creating the Lense–Thirring effect on the exact relativistic Kerr geometry. The value of β is given by

$$\beta = \frac{r_{\rm in}}{r_1} - 1, \quad (3)$$

where the last stable orbit

$$r_{\rm in} = \{3 + Z_2 \mp [(3-Z_1)(3+Z_1+2Z_2)]^{1/2}\}r_{\rm g}, \quad (4)$$

with

$$Z_1 = 1 + (1-a^2)^{1/3}[(1+a)^{1/3} + (1-a)^{1/3}], \quad (5)$$

$$Z_2 = \sqrt{3a^2 + Z_1^2}. \quad (6)$$

Note that the upper minus and lower plus signs in Eq. (4) correspond to co-rotation ($a > 0$) and counter-rotation ($a < 0$), respectively. It is clear that the potential (1) corresponds to the free-fall 3-dimensional acceleration

$$\boldsymbol{A} = -\frac{GM}{r^{2-\beta}(r-r_1)^{\beta}}\frac{\boldsymbol{r}}{r}. \quad (7)$$

As claimed in Ref. [21], the potential has three basic properties: (i) in the nonrotating case, the free-fall acceleration is exactly the PW potential $\phi_{\rm PW} = -GM/(r-2r_{\rm g})$ of the object; (ii) the free-fall acceleration becomes infinite as r approaches the event horizon of the black hole; (iii) the position of the extremum of the boundary condition function is the same as that of the last stable circular orbit in the exact relativistic Kerr metric. In addition, the potential compared with the relativistic counterpart can reproduce the accretion disk structure to an accuracy of about 10%–20%. In addition, it was shown in Table 1 of Ref. [22] that the values of the marginally bound orbit in both the ABN potential and the Kerr geometry for the range of $a \in (-1, 1)$ are in a good agreement with each other. It should be emphasized that such a good agreement is based on the choice of lower plus sign in Eq. (4) for the counter-rotation case.[20] In short, unlike the Newtonian potential $\phi_{\rm N} = -GM/r$ of the main object, the simple potential $\phi_{\rm ABN}$ can capture the essence of the general relativistic effects from the exact relativistic Kerr metric. It is a certain approximation (incompletely equivalent) to the Kerr geometry.

Seen from the above-mentioned points, this treatment is called simple general relativity. In this sense, one can easily understand some general relativistic effects from the framework of Newtonian mechanics. Then it is convenient to discuss the superposition of several Newtonian gravitational fields because the Newtonian theory of gravity is a kind of linear gravitational theory. Namely, the superposition is regarded as a linear combination of these gravitational fields or potentials. Except for the black hole with the ABN pseudo-Newtonian potential, there are halos far from the black hole, which are given by the quadrupolar moment. The halos have the following Newtonian potential

$$\psi = Qr^2 P_2(\cos\theta), \quad (8)$$

where $P_2(\cos\theta) = (3\cos^2\theta - 1)/2$ with $\cos\theta = z/r$ being the second Legendre polynomial. The quadrupolar parameter Q has two distinct situations of $Q > 0$ and $Q < 0$. The first case is related to the oblate deformation like oblate halos, and the second case to the prolate deformation like prolate halos. In the cylindrical coordinates (ρ, φ, z) with $r = \sqrt{\rho^2 + z^2}$, Eq. (8) is rewritten as

$$\psi = \frac{1}{2}Q(2z^2 - \rho^2). \quad (9)$$

The gravity between the black hole and the halos is governed by the linear superposition of the two potentials in the manner

$$\Phi = \phi_{\rm ABN} + \psi. \quad (10)$$

The motion of a test particle in the superposed field is described by a nondimensional Hamiltonian[23]

$$H = \frac{1}{2}(p_\rho^2 + p_z^2) + \frac{1}{2}\frac{L^2}{\rho^2} + \Phi. \quad (11)$$

It is worth noting that the considered superposed field is axially symmetric. In this sense, there is a conserved angular momentum L of the particle. Additionally, a series of nondimensional operations are made by taking $r \leftrightarrow r/r_{\rm g}$, $p_z \leftrightarrow p_z/(\mu c)$, $t \leftrightarrow ct/r_{\rm g}$, $L \leftrightarrow L/(\mu c r_{\rm g})$, etc., where μ represents the particle mass. Meanwhile, both the gravitational parameter GM in Eqs. (1) and (7) and the factor $r_{\rm g}$ in Eqs. (2) and (4) should be replaced with 1. In terms of the system (11), we obtain the effective potential

$$V_{\rm eff} = \frac{1}{2}\frac{L^2}{\rho^2} + \Phi. \quad (12)$$

It should be emphasized particularly that the use of the ABN pseudo-Newtonian potential instead of the general relativistic solution lies in not only the simplification of solving the geodesic equations but also that of obtaining the superposed gravitational field between the ABN pseudo-Newtonian potential and quadrupolar halos. As claimed above, the ABN potential can capture the essence of the general relativistic effects given by the exact relativistic Kerr metric. In addition, we wonder whether the ABN pseudo-Newtonian potential has basic properties similar to those of the general relativistic solution from a dynamical point of view. In other words, let us provide some insights into the dynamics of particles moving in the superposed field (11).

3. Regular and chaotic dynamics of test particles in the superposed field

In this section, we focus on analyzing the stability of the circular orbits of test particles in the superposed gravitational field. Above all, we pay more attention to the dynamical behaviors of generic orbits by using different methods to detect chaos from order. Moreover, a transition to chaos on a certain parameter is also explored.

3.1. Circular orbits

Because the gravity of the black hole is a central force and the quadrupole possess a reflection symmetry on the equatorial plane $z = 0$, the stable circular orbits are only limited to the plane. In this case, we have $r = \rho$ and $p_z = 0$, and further obtain conditions for the existence of circular orbits as follows:

$$\begin{cases} \dot{r} = 0, \\ \dot{p_r} = 0. \end{cases} \tag{13}$$

It can be inferred that

$$L^2 = r^{\beta+1}(r - r_1)^{-\beta} - Qr^4. \tag{14}$$

In addition, the condition for the stability of circular orbits should satisfy the relation

$$\frac{\partial^2 V_{\rm eff}}{\partial r^2} \geq 0. \tag{15}$$

In the light of Eqs. (14) and (15), the stability criterion of circular orbits is reduced to

$$C(r) = r^{\beta-3}(r - r_1)^{-(\beta+1)}[r - r_1(\beta + 1)] - 4Q \geq 0. \tag{16}$$

Especially for the nonrotating case with $a = 0$, Eq. (16) is rewritten as

$$r \geq 6 + 4Qr(r - 2)^3. \tag{17}$$

Only when $C(r) = 0$, is the innermost stable circular orbit obtained for a given parameter pair of (a, Q). Then, it is obvious to see from Eq. (17) that in the absence of the matter of halos, the radius of the innermost stable circular orbit in a Schwarzschild metric is only 6. In addition, the radii of the innermost stable circular orbits should be smaller than 6 for the prolate halos, but larger for the oblate halos. Furthermore, the test particles are also affected by the perturbed force from the matter of halos with $Q \neq 0$. Given the maximum counter-rotation $a = -1$, the radii of the innermost stable circular orbits satisfy $r = 9 + 4Qr^{-5}(r - 1)^9$. This implies that the radii are larger than 9 for the oblate halos, but smaller for the prolate halos. As far as other situations of $a \neq 0, -1$ and $Q \neq 0$ are concerned, it is not difficult to discuss the innermost stable circular orbits from an analytical point of view. However, the perturbation Q, which is in an order of magnitude of 10^{-5} or so, is too small to have a great influence on the radii of the innermost stable circular orbits. The spin angular momentum a plays an important role in dominating the innermost stable circular orbits. In this sense, it is suggested that the radii of the innermost stable circular orbits take the approximation $R_{\rm ISCO} = r_{\rm in} + \varepsilon$ with $\varepsilon = -C/C'|_{r=r_{\rm in}}$. In Fig. 1, this approach is confirmed to be in good agreement with numerical results as $|Q|$ is small. In addition, the dependence of $R_{\rm ISCO}$ on the spin angular momentum a for a given value

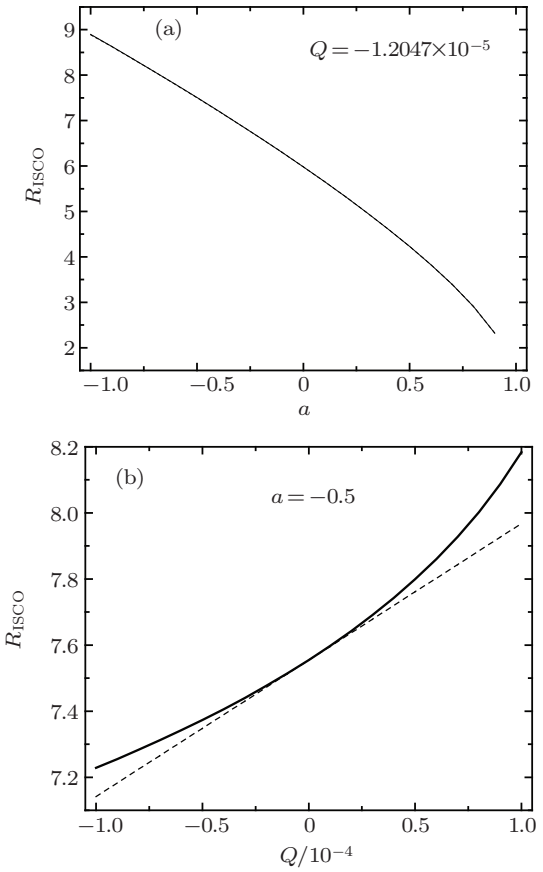


Fig. 1. Dependences of the radii $R_{\rm ISCO}$ of the innermost stable circular orbits on (a) the spin angular momentum a and (b) the quadrupolar parameter Q. The dashed lines are the radii from the approximate method, and the straight lines represent the ones from the Newton iteration method. The two methods provide almost the same results for small values of $|Q|$.

of the quadrupolar moment Q (or the dependence of $R_{\rm ISCO}$ on the quadrupolar moment Q for a given value of the spin angular momentum a) is shown clearly. It is easy to find that $R_{\rm ISCO}$ decreases when a runs from the maximum counter-rotating case to the limit case of $a = 1$. On the contrary, it increases as the halos change from the prolate case with $Q = -1.0 \times 10^{-4}$ to the oblate case with $Q = 1.0 \times 10^{-4}$.

The above discussions demonstrate that such a weak perturbation from the halos, except for the spin angular momentum of the rotating black hole, does not exert a dramatic influence on both the stability and radii of the innermost stable circular orbits of test particles. What about generic orbits? It is necessary to perform a more detailed numerical investigation in order to answer this question.

3.2. Generic orbits

As is well known, the exact relativistic Kerr field is integrable because there are four integrals of motion, including the energy of a test particle, the angular momentum, the rest mass, and the Carter constant. We will focus on the question of whether the ABN pseudo-Newtonian potential for modeling the Kerr field can preserve this integrable property.

The system (11) with potential ψ turned off is rewritten in the spherical coordinates (r, ϑ, φ) ($x = r\cos\varphi\sin\vartheta$, $y = r\sin\varphi\sin\vartheta$, and $z = r\cos\vartheta$)

$$\mathcal{H} = \frac{1}{2}\left(p_r^2 + \frac{p_\varphi^2}{r^2\sin^2\vartheta} + \frac{p_\vartheta^2}{r^2}\right) + \phi_{\rm ABN}(r). \tag{18}$$

Its Hamilton–Jacobi equation is

$$\frac{\partial S}{\partial t} + \frac{1}{2}\left[\left(\frac{\partial S}{\partial r}\right)^2 + \frac{1}{r^2\sin^2\vartheta}\left(\frac{\partial S}{\partial \varphi}\right)^2 + \frac{1}{r^2}\left(\frac{\partial S}{\partial \vartheta}\right)^2\right] + \phi_{\rm ABN}(r) = 0. \tag{19}$$

Since t and φ do not explicitly appear in Eq. (19), there are two integrals: the energy $E = \mathcal{H}$ and the angular momentum $L = p_\varphi$ of the particle. Then the generating function S is supposed to have a separable variable form $S = -Et + L\varphi + S_1(r) + S_2(\vartheta)$ such that

$$r^2\left[2E - \left(\frac{{\rm d}S_1}{{\rm d}r}\right)^2 - 2\phi_{\rm ABN}(r)\right] \equiv \left(\frac{{\rm d}S_2}{{\rm d}\vartheta}\right)^2 + \frac{L^2}{\sin^2\vartheta}. \tag{20}$$

The identical relation is always true for any r and ϑ if and only if the left-hand side and the right-hand side are both equal to the same constant. When the constant is labeled as κ, we have

$$\kappa = r^2\left[2E - \left(\frac{{\rm d}S_1}{{\rm d}r}\right)^2 - 2\phi_{\rm ABN}(r)\right], \tag{21}$$

$$\kappa = \left(\frac{{\rm d}S_2}{{\rm d}\vartheta}\right)^2 + \frac{L^2}{\sin^2\vartheta}. \tag{22}$$

Obviously, $S_1(r)$ and $S_2(\vartheta)$ can be solved analytically from a theoretical point of view, respectively. Considering $p_r = \partial S/\partial r$ and $p_\vartheta = \partial S/\partial\vartheta$, we rewrite Eqs. (21) and (22) as

$$r^2[2E - p_r^2 - 2\phi_{\rm ABN}(r)] = \kappa, \tag{23}$$

$$p_\vartheta^2 + \frac{L^2}{\sin^2\vartheta} = \kappa. \tag{24}$$

Therefore, the existence of the third constant κ (note that Eqs. (23) and (24) are not two independent integrals of motion, and only one of them can be chosen as the third integral) must lead to the integrability of the pseudo-Newtonian Kerr field. The integrability can be also seen from the fact that the ABN gravitational potential is symmetric with respect to the origin point $O(0, 0, 0)$, namely, the description of a general spherically symmetric rotating black hole.

If a small perturbation from the halos is added, the non-separability of variables in the superposed system occurs at once. This can be seen clearly from the following expression:

$$\chi = r^2[2E - p_r^2 - 2\phi_{\rm ABN}(r)] = p_\vartheta^2 + \frac{L^2}{\sin^2\vartheta} + Qr^4(2\cos^2\vartheta - \sin^2\vartheta). \tag{25}$$

Although we cannot confirm the absence of the third constant χ of motion now because the Hamilton–Jacobi method depends on the choice of variables, we can use numerical tools to show the existence of chaotic bound orbits in the superposed field. This implies that there is no additional constant χ in general except for the energy and angular momentum of a particle. In this sense, system (11) becomes near-integrable or completely nonintegrable. In other words, the small perturbation does destroy the integrability of the pseudo-Newtonian Kerr field. In what follows, it is necessary to evaluate the contribution of the perturbation to the possible existence of chaos in the system with the help of different chaos indicators.

3.2.1. Poincaé sections

The method of Poincaé sections can show the intersection of a trajectory with the section surface in

phase space. It is the most intuitive technique to clearly describe the dynamical structure of the whole phase space on a 2-dimensional plane when the number of dimensions of the phase space of a system minus the number of all integrals of motion is smaller than 3.[24] Qualitative properties of the system can be shown in terms of three aspects: (i) the motion is strictly periodic if one or more isolated points stay on the section surface; (ii) one or more tori on the plane indicate the quasi period or the regularity of orbits; (iii) a set of random continuous points distributed on the plane signify the chaoticity of orbits. The method is very suitable for the study of system (11) due to the existence of the energy integral (11) in a 4-dimensional phase space.

First, let us consider two special cases, the non-rotating black holes with the Newtonian potential $\phi_{\rm N}$ and the PW pseudo-Newtonian potential $\phi_{\rm PW}$. The latter case corresponds to $a = 0$, $r_1 = 2$, and $\beta = 2$ in Eq. (1) or Eq. (7). Here the PW potential is used to approximately mimic the Schwarzschild spacetime. When the other dynamical parameters $E = -0.025$, $L = 3.8$, and $Q = -1.2047 \times 10^{-5}$ are chosen, we apply a numerical integration scheme to plot the point (ρ, p_ρ), where the particle crosses the Poincaé section (i.e., the equatorial plane $z = 0$) with $p_z > 0$. As shown in Fig. 2(a), the phase space of the system composed of the Newtonian black hole and the prolate halos is full of all Kolmogrov–Arnold–Moser (KAM) tori. This implies that the dynamics is typically regular under the considered parameters. However, there is chaos only when the Newtonian potential is replaced with the PW pseudo-Newtonian potential. Because of this, we can say that the general relativistic effects from the PW potential are an important source of chaos and must enhance its strength.

Then let us provide some insights into the dynamics of the ABN pseudo-Newtonian rotating black hole plus the halos. The dynamical parameters are the same as those in Fig. 2, but the spin angular momentum a of the rotating black hole is given in various admissible values. Several points can be concluded from Fig. 3. (i) The dynamical structure of the phase space is completely different when the absolute value of the spin angular momentum a changes. (ii) The dynamical structures are also different for the cases of counter-rotation and co-rotation. It is worth emphasizing that the bounded region of motion becomes much smaller in the counter-rotating system than in the co-rotating system. When the particle moves out from the bounded region of motion, its motion is unstable. This means that the counter-rotating system is more unstable. (iii) Chaos occurs mainly for smaller values of $|a|$. In particular, chaos is absent for the maximum counter-rotating case either (not plotted in Fig. 3).

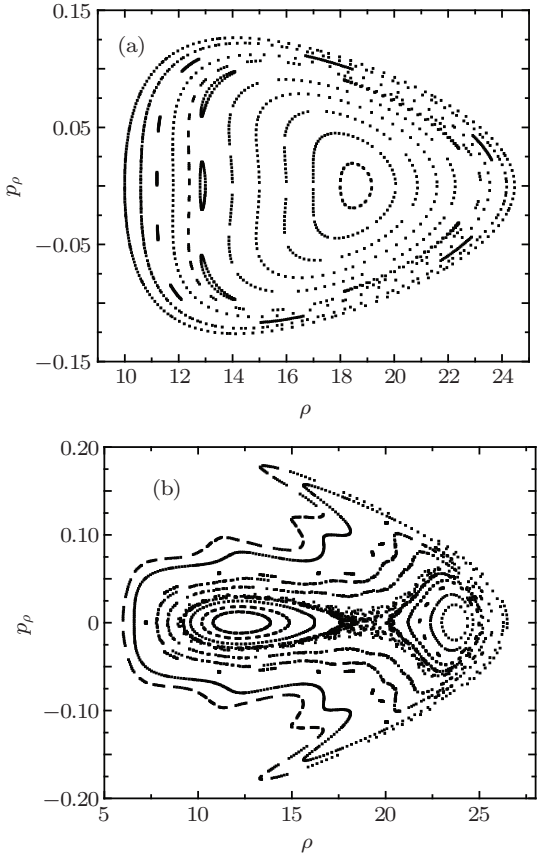


Fig. 2. Poincaé section on the $z = 0$ plane with $p_z > 0$ for two gravitational systems: (a) the Newtonian potential $\phi_{\rm N}$ plus the quadrupolar halos; (b) the PW potential $\phi_{\rm PW}$ plus the quadrupolar halos. The two panels use the same parameters: $a = 0$, $E = -0.025$, $L = 3.8$, and $Q = -1.2047 \times 10^{-5}$.

Now the effect of the quadrupolar parameter Q is mainly explored with the help of the method of Poincaé sections. The parameters E and L in Figs. 4(a)–4(c) are still taken from Fig. 3, but $a = 0.1$ is fixed and Q has different values. When the oblate halos are used instead of the prolate ones in Fig. 3(b), there is no chaos in Fig. 4(a). This shows that the prolate halos more easily yield chaos than the oblate ones. The comparison between Figs. 4(b) and 4(c) also supports this fact.

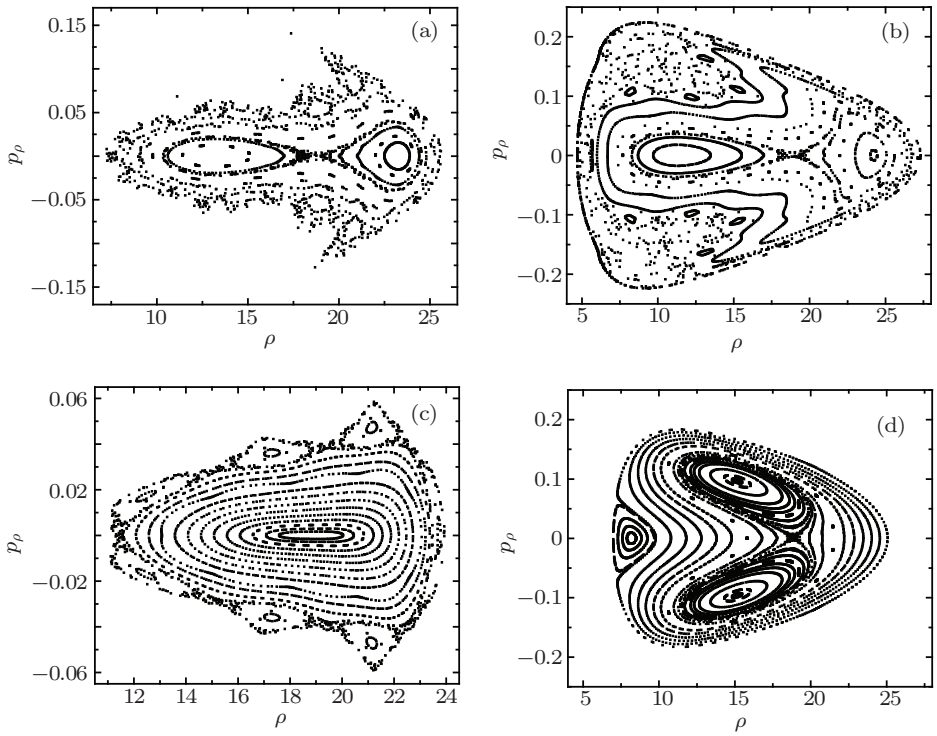


Fig. 3. Poincaé section on the $z = 0$ plane with $p_z > 0$ for the ABN potential $\phi_{\rm ABN}$ plus the quadrupolar halos with the rotation parameter (a) $a = -0.1$, (b) $a = 0.1$, (c) $a = -0.5$, and (d) $a = 0.5$. All the panels have the same parameters: $E = -0.025$, $L = 3.8$, and $Q = -1.2047 \times 10^{-5}$.

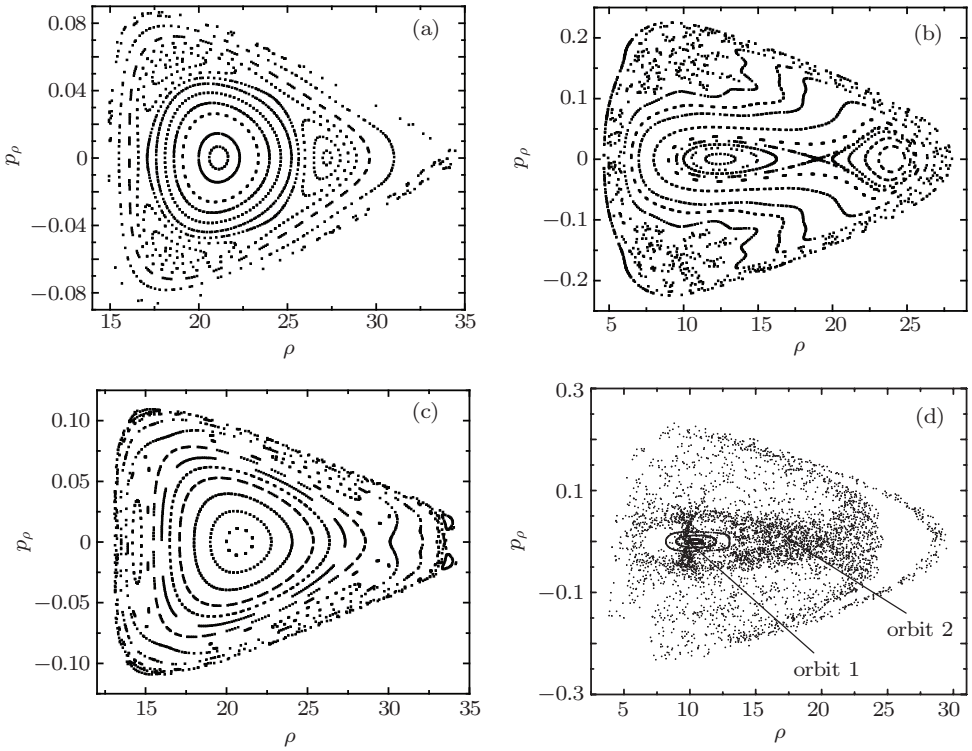


Fig. 4. Poincaé section on the $z = 0$ plane with $p_z > 0$ for the ABN potential $\phi_{\rm ABN}$ plus the quadrupolar halos with the quadrupolar parameter (a) $Q = 1.2047 \times 10^{-5}$, (b) $Q = -1 \times 10^{-5}$, (c) $Q = 1 \times 10^{-5}$, and (d) $Q = -1.2047 \times 10^{-5}$. In Figs. 4(a)–4(c), $E = -0.025$, $L = 3.8$, and $a = 0.1$. In Fig. 4(d), $E = -0.0223573$, $L = 3.8$, and $a = 0.04$.

In short, the method of Poincaé sections can describe the dynamical dependence on the parameters of Q, a, and E. The quadrupolar parameter Q destroys the integrability of the ABN pseudo-Newtonian potential so that test particles in the superposed field have richer dynamical behaviors. Chaos does not exist for small values of $|Q|$. It is further found that chaos occurs more easily for the prolate halos than for the oblate ones. Moreover, it is clear that the sign of the spin angular momentum a of the rotating black hole has a great influence on the structure of phase space of the superposed field. The bounded regions of motion become much smaller in the counter-rotating system than in the co-rotating system. This means that the counter-rotating system is more unstable. It is worth noting that chaos occurs mainly for smaller values of $|a|$. If the energy E of the particle increases, the chaos becomes stronger, as shown in Fig. 4(d). Although the method of Poincaé sections is a good means to draw the global structure of phase space for a group of fixed parameters, it may be very inconvenient to trace a dynamical sensitivity to the variation of all the parameters. In this sense, it is necessary to employ other better qualitative methods.

3.2.2. Fast Lyapunov indicators

Besides the method of Poincaé sections, there are a number of methods to find chaos. For example, the Melnikov's method,[25] the Lyapunov exponents,[26,27] the power spectrum analysis,[28] the fast Lyapunov indicators,[29] and the 0–1 test algorithm[30] are often used.

The maximum Lyapunov exponent is a common qualitative method to distinguish chaos from order. It is an important quantitative indicator which measures the rate of the exponential divergence between neighboring trajectories in the phase space. A tangent vector $\xi(t)$ (i.e., the solution of the variational equations with respect to the equations of motion) at time t with the tangent vector $\xi(0)$ at the starting time is used as a basic definition of the indicator in the form

$$\lambda = \lim_{t\to\infty} \frac{1}{t} \ln \frac{|\xi(t)|}{|\xi(0)|}. \tag{26}$$

This is the variational method for computing the Lyapunov exponent, which requires renormalization from time to time so that overflow can be avoided. A bounded system is chaotic if $\lambda > 0$, but regular if $\lambda = 0$. The Lyapunov exponents of two orbits in Fig. 4(d) are shown in Fig. 5. The initial conditions of orbit 1 are $\rho = 10$, $z = 0$, $p_z = 0$, and $p_\rho > 0$, and orbit 2 has the same initial conditions as orbit 1 except $\rho = 17.04$ and p_ρ. Although the method of Poincaé sections has confirmed that orbits 1 and 2 are respectively regular and chaotic, the Lyapunov exponents do not seem to distinguish between the two types of orbits. This is because it usually takes a rather long time to obtain the limit values of the Lyapunov exponents, and the Lyapunov exponents are not a sensitive indicator for weak chaotic motion.

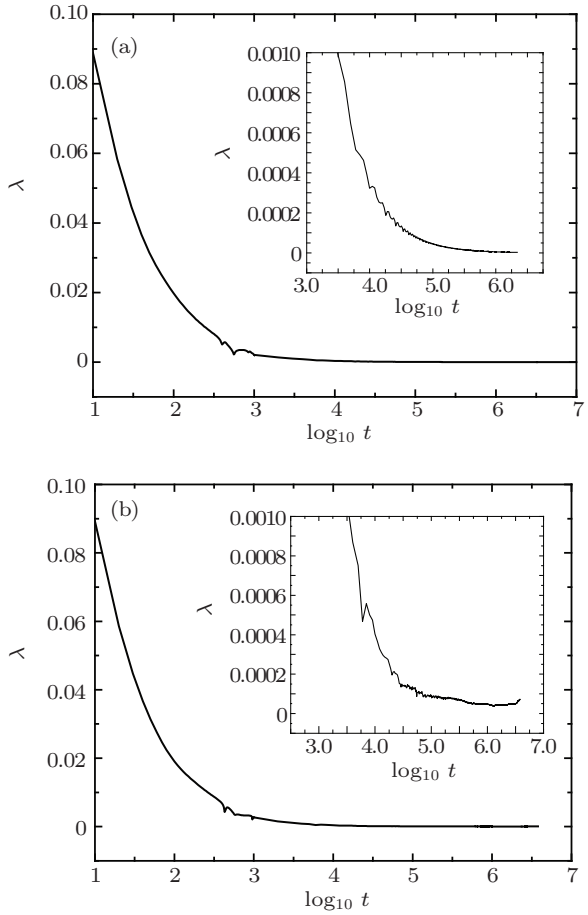


Fig. 5. Lyapunov exponent λ for the (a) orbit 1 and (b) orbit 2 in Fig. 4(d).

However, the method of power spectrum analysis can describe the dynamical feature of the two orbits. As shown in Fig. 6, the discrete spectra of orbit 1 indicate its regularity, while the continuous spectra of orbit 2 signify its chaoticity. The power spectrum analysis is based on Fourier techniques, which can analyze the feature of signals in terms of a distribution of frequency.

It should be noticed that the fast Lyapunov indicators are regarded as being more sensitive to chaos. They were proposed firstly in Ref. [29]. Then

Froeschlé and Lega[31] modified the fast Lyapunov indicator as follows:

$$\Lambda(t) = \log_{10} |\xi(t)|. \tag{27}$$

The common logarithm of the length of the deviation vector stretches exponentially with time $\log_{10} t$ for a chaotic orbit, but linearly for an ordered one. In addition, the value of FLI for the chaotic motion is much larger than for the ordered motion. These characteristics can be used to distinguish between ordered and chaotic cases. As a variant of this indicator, the two-particle method, which adopts the distance between two nearby trajectories rather than the length of the tangent vector, was developed in Ref. [32]. This method has been applied, for instance, in Refs. [33]–[35].

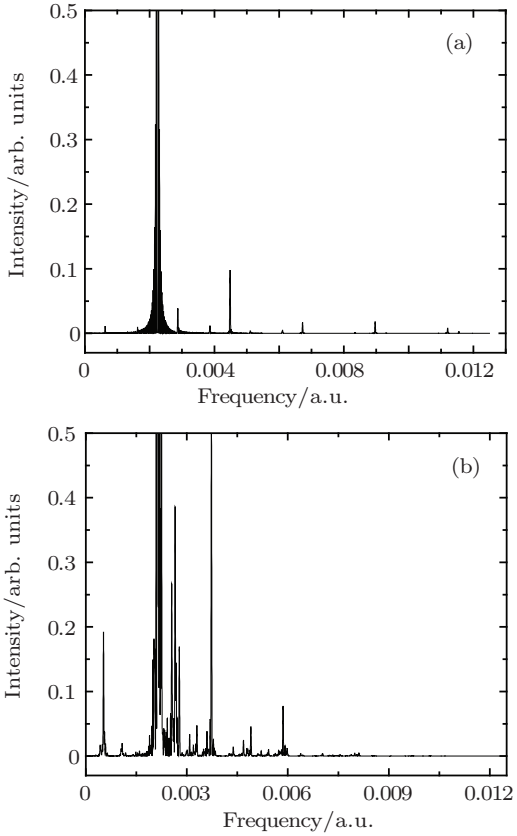


Fig. 6. Power spectra of (a) orbit 1 and (b) orbit 2.

Seen from Fig. 7, the FLIs of orbit 2 are much larger than those of orbit 1 as the integration time spans a range of 10^5. This shows that orbit 2 is chaotic, but orbit 1 is regular. Obviously, the FLI method, compared with that of Lyapunov exponents, is a quicker and more efficient tool for detecting chaos from order. Because of its advantages, it will be used to investigate the dependence of the regular and chaotic dynamics on a single parameter.

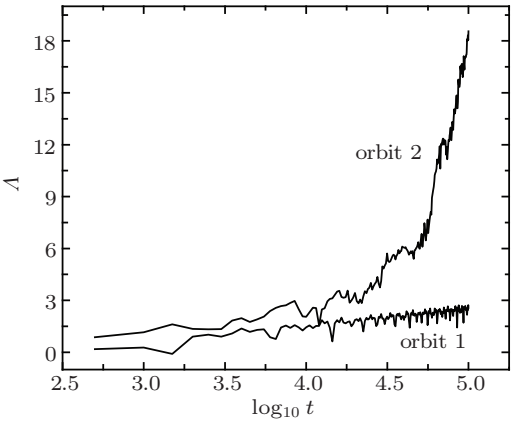


Fig. 7. Fast Lyapunov indicators of (a) orbit 1 and (b) orbit 2.

Let initial conditions be fixed and one of the parameters E, a, and L changes. Once such a parameter is given, its corresponding orbit is also determined. Then the final FLI of the orbit is obtained when the integration time $t = 10^5$. Figure 8(a) tells us the relationship between the FLIs and the energy E. It is discovered by many numerical experiments that the orbits with a FLI larger than 7 are chaotic, while the ones with a FLI smaller than 7 are ordered. As is expected, a dynamical sensitivity to chaos occurs when the energy reaches a certain threshold value. Additionally, it is easy to see that the larger the energy is, the stronger the chaos becomes. In addition, the dynamical dependence of the FLIs on the spin angular momentum a in Figs. 8(b) and 8(c) seems to show that chaos tend to occur with slightly more probability for a positive a than a negative a. Now it can be concluded from Figs. 3, 8(b), and 8(c) that there are more unstable, unbounded orbits in the counter-rotating system than in the co-rotating system, but chaos occurs slightly easier in the co-rotating system than in the counter-rotating system. This result seems to be inconsistent with that in Ref. [22]. As claimed in the article, " negative values of a are associated to a larger Lyapunov exponent when compared with their correspondent positive values. It means that two neighbour orbits separate from each other faster in the counter-rotating system than in the co-rotating system, meaning that the counter-rotating system is more unstable". The word "unstable" means a larger Lyapunov exponent of a chaotic bound orbit. That is to say, the chaos of bounded orbits becomes stronger in the counter-rotating system than in the co-rotating

system. It is different from the word "unstable" mentioned in Section 3.2.1, which means the unboundness of orbits. In our opinion, there is actually no explicit conflict between these different results. Without any doubt, they are all correct. This is because dynamical models and a combination of all the initial conditions and parameters in the present paper and Ref. [22] are completely different. Moreover, it is proved again that chaos does mainly occur for smaller values of $|a|$, and it does not exist for the maximum counter-rotating case. As an illustration, Ref. [9] concluded that "the dragging effects of the spacetime by a rotating black hole weaken the chaotic properties and generate regular trajectories for some sets of initial parameters, while the chaotic properties dominate on the trajectories for slowly rotating black hole cases". This shows that the ABN potential in the present paper and the exact relativistic Kerr geometry in Ref. [9] are equivalent to a great degree from the point of view of the rotating parameters weakening the chaotic properties.

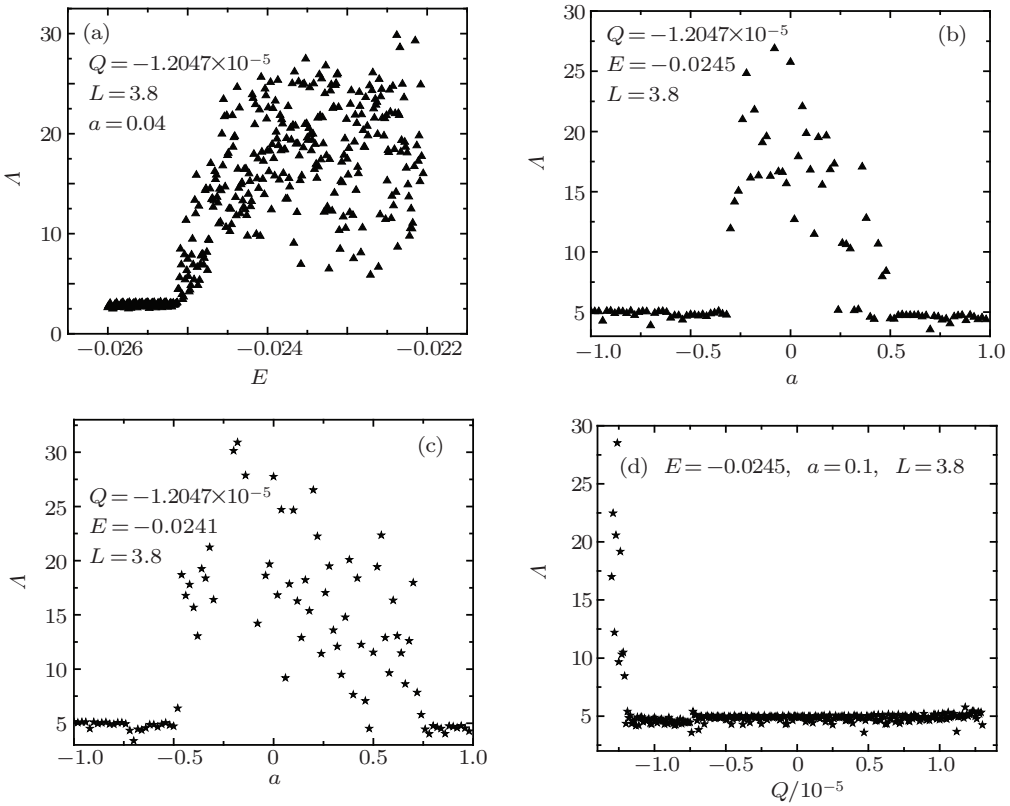


Fig. 8. Fast Lyapunov indicator as a function of (a) E, (b) and (c) a, and (d) Q.

The dependence of the FLIs on the quadrupolar parameter Q, as shown in Fig. 8(d), supports the fact that the prolate halos can lead to chaos more easily than the oblate ones. In a similar way, we can conclude that it is slightly easier to produce chaos in the co-rotating system than in the counter-rotating system, and a larger energy increases the strength of chaos.

In summary, the FLI method qualitatively coincides with that of the Poincaé sections in describing the dependence on a single parameter.

3.2.3. Qualitative interpretations

Some of the above results are explained here. As shown clearly in Section 2, a test particle is mainly subject to the action of the gravity of the central compact object. Additionally, the perturbation from the halos also affects its motion. If the gravity of the central body is too strong and the perturbation force is extremely weak, the particle's dynamics is completely dominated by the gravity. In this sense, system (11) maintains the properties of the ABN potential. That is to say, KAM tori in the ABN potential are not destroyed by such a weak perturbation. In other words,

the occurrence of chaos is impossible. Only when the perturbation becomes large enough, is it possible for chaos to occur.

Without doubt, chaos should become more dramatic as the energy of the system increases. This is because the semimajor axis A gets larger so that the dominant force is weakened, as can be seen from the approximate to the Kepler energy $K = -GM/(2A)$. In addition, the distinct dynamical structures for the co-rotating and counter-rotating cases are due to the choice of two signs in Eq. (4). In the limit of the spin parameter $a \to -1$ for the counter-rotating case, the function $[r/(r-r_1)]^{\beta}$ in acceleration (7) is a monotonically increasing function of $-a$ ($a < 0$) for a fixed radius r so that the dominant force gets stronger. In the limit of the spin parameter $a \to 1$ for the co-rotating case, the ABN potential tends to be the Kepler potential. As a result, the relativistic effects disappear gradually. These points show that the rotating parameters can weaken the chaotic properties.

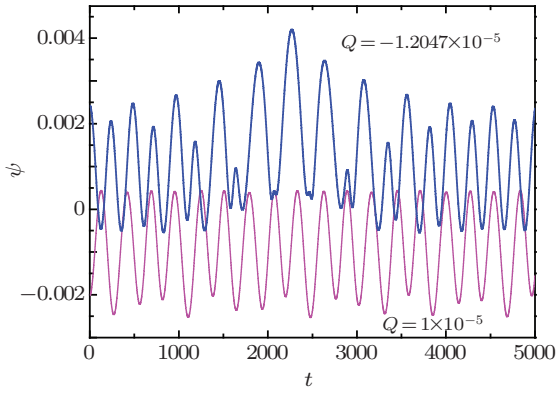


Fig. 9. (colour online) Evolution of the potentials (9) for the prolate and oblate halos in Fig. 8(d) with time. The case of $Q = -1.2047 \times 10^{-5}$ corresponds to the chaoticity of the superposed system, and the case of $Q = 1 \times 10^{-5}$ corresponds to the regularity of the orbit.

Finally, let us consider why chaos occurs more easily for prolate halos than for the oblate ones. This can be understood simply from Fig. 9. The potential ψ of the prolate halo is positive in most cases during its evolution, while that of the oblate halo is always negative. When they are respectively added to the ABN negative potential, the superposed system is more unstable for the former case, that is, it is easier for chaos to appear in the former case. This can be also explained with the help of the scalar Virial theorem.[36] As for the theorem states, a necessary condition for stability is $\langle T\rangle + \langle K\rangle = 0$, where $\langle T\rangle$ is the time average of the kinetic energy and $\langle K\rangle$ denotes the time average of the Kepler energy. If the average of total energy $\langle E\rangle = \langle T\rangle + \langle \phi_{\rm ABN}\rangle + \langle \psi\rangle$ of the superposed system is given, $\langle T\rangle$ should be smaller for $\langle \psi\rangle > 0$ than for $\psi \equiv 0$. This leads to the increase of $\langle K\rangle$, namely, the increase of the semimajor axis. Therefore, the gravity of the central body gets weaker and the perturbation force becomes stronger so that chaos tends to occur for the prolate halos.

4. Conclusion

The ABN potential as a simple general relativity is a certain approximation to some general relativistic effects of the exact relativistic Kerr spacetime. It is typically integrable due to the existence of three constants of motion, but non-integrable when the quadrupolar halos are added because there is no additional constant of motion except the constants associated with the energy and the angular momentum of a test particle in the superposed field.

The weak perturbation from the halos, except the spin angular momentum of the rotating black hole, does not have a great effect on both the stability and the radii of the innermost stable circular orbits of test particles. However, it gives the generic orbits richer dynamical behaviors. The investigation into them lies mainly in the understanding of the dynamical dependence on the two parameters: the quadrupolar parameter Q of the halos and the spin angular momentum a of the spinning black hole. It is found that chaos mainly occurs for small values of $|a|$, and does not exist for the maximum counter-rotating case under some sets of initial conditions and other parameters. It is proved in a simple way that the rotating parameter in the ABN potential, like in the exact relativistic Kerr geometry, weakens the chaotic properties. In addition, the counter-rotating system is more unstable than the co-rotating system. In addition, chaos does not exist for small values of $|Q|$ at all. In particular, chaos more easily occurs for prolate halos than for the oblate ones.

This paper has shown that the ABN pseudo-Newtonian potential and the exact relativistic Kerr spacetime are almost the same in describing the rotating parameters which weaken the chaotic properties. In this way, the study of many complicated relativistic dynamical problems will become an easier task.

References

[1] Chen J H and Wang Y J 2003 *Chin. Phys.* **12** 836
[2] Chen J H and Wang Y J 2004 *Chin. Phys.* **13** 583

[3] Chen J H and Wang Y J 2005 *Chin. Phys.* **14** 1282
[4] Chen J H and Wang Y J 2006 *Chin. Phys.* **15** 1705
[5] Zhong S Y and Wu X 2011 *Acta Phys. Sin.* **60** 090402 (in Chinese)
[6] Contopoulos G, Voglis N and Efthymiopoulos C 1999 *Celest. Mech. Dyn. Astron.* **73** 1
[7] Vieira W M and Letelier P S 1997 *Phys. Lett.* A **228** 22
[8] Wu X and Zhang H 2006 *Astrophys. J.* **652** 1466
[9] Takahashi M and Koyama H 2009 *Astrophys. J.* **693** 472
[10] Suzuki S and Maeda K I 1997 *Phys. Rev.* D **55** 4848
[11] Verhaaren C and Hirschmann E W 2010 *Phys. Rev.* D **81** 124034
[12] Hartl M D 2003 *Phys. Rev.* D **67** 024005
[13] Wu X and Xie Y 2010 *Phys. Rev.* D **81** 084045
[14] Wu X 2010 *Res. Astron. Astrophys.* **10** 211
[15] Ma D Z, Wu X and Zhong S Y 2009 *Res. Astron. Astrophys.* **9** 1185
[16] Paczyński B and Wiita P 1980 *Astron. Astrophys.* **88** 23
[17] Guéron E and Letelier P S 2001 *Astron. Astrophys.* **368** 716
[18] Steklain A F and Letelier P S 2006 *Phys. Lett.* A **352** 398
[19] Semerák O and Karas V 1999 *Astron. Astrophys.* **343** 325
[20] Mukhopadhyay B 2002 *Astrophys. J.* **581** 427
[21] Artemova I V, Björnsson G and Novikov I D 1996 *Astrophys. J.* **461** 565
[22] Steklain A F and Letelier P S 2009 *Phys. Lett.* A **373** 188
[23] Wang Y and Wu X 2011 *Commun. Theor. Phys.* **56** 1045
[24] Xu J, Wu X and Ma D Z 2010 *PRAMANA - J. Phys.* **74** 907
[25] Di G H, Xu Y, Xu W and Gu R C 2011 *Acta Phys. Sin.* **60** 020504 (in Chinese)
[26] Feng C W, Cai L, Kang Q and Zhang L S 2011 *Acta Phys. Sin.* **60** 030503 (in Chinese)
[27] Zhang X D and Cai L J 2011 *Acta Phys. Sin.* **60** 110511 (in Chinese)
[28] Binney J and Spergel D 1982 *Astrophys. J.* **252** 308
[29] Froeschlé C, Lega E and Gonczi R 1997 *Celest. Mech. Dyn. Astron.* **67** 41
[30] Sun K H, Liu X and Zhu C X 2010 *Chin. Phys.* B **19** 110510
[31] Froeschlé C and Lega E 2000 *Celest. Mech. Dyn. Astron.* **78** 167
[32] Wu X, Huang T Y and Zhang H 2006 *Phys. Rev.* D **74** 083001
[33] Li R and Wu X 2010 *Acta Phys. Sin.* **59** 7135 (in Chinese)
[34] Li R and Wu X 2011 *Eur. Phys. J. Plus* **126** 73
[35] Wang Y Z and Wu X 2011 *Class. Quantum Grav.* **28** 025010
[36] Binney J and Tremaine S 1987 *Galactic Dynamics* (Princeton: Princeton University Press) pp. 10–400